Nuclear charge radii and shape evolution of Kr and Sr isotopes with the deformed relativistic Hartree-Bogoliubov theory in continuum

X. Y. Zhang (张晓燕),[1] Z. M. Niu (牛中明) ●,[1,*] W. Sun (孙玮),[2,3] and X. W. Xia (夏学伟)[4]

[1]*School of Physics and Optoelectronic Engineering, Anhui University, Hefei 230601, China*
[2]*School of Physical Science and Technology, Southwest University, Chongqing 400715, China*
[3]*Department of Physics and Astronomy, University of Notre Dame, Notre Dame, Indiana 46556, USA*
[4]*School of Physics and Electronic Engineering, Center for Computational Sciences, Sichuan Normal University, Chengdu 610068, China*

The deformed relativistic Hartree-Bogoliubov theory in continuum (DRHBc) is employed to study the ground-state properties of Kr and Sr isotopes. Based on the constrained DRHBc calculations, it is found that Kr and Sr isotopes with $N = 50$ are spherical, while the nuclei just away from $N = 50$ generally have soft potential energy curves. Further moving along the isotopic chains in both neutron-rich and neutron-deficient directions, there are generally two minima at oblate and prolate sides for nuclear potential energy curves, where possible candidates for shape coexistence are found. The dynamical correlations are crucial to describe the properties of nuclei with soft potential energy curves or shape coexistence, e.g., the binding energies, two-neutron separation energies, deformations, and charge radii, which are considered with the two-dimensional collective Hamiltonian method. In addition, the constrained DRHBc calculations would be helpful to distinguish the oblate or prolate shape for the nuclei with deformation $|\beta_2| \gtrsim 0.3$ by combining with the experimental charge radii and absolute values of deformations.

I. INTRODUCTION

Nuclear charge radius is a basic physical quantity in nuclear physics, which can be used to extract various nuclear structure information, e.g., halo phenomena [1], shape evolution and shape coexistence [2,3], and nuclear magic numbers [4,5]. It also provides a stringent test and challenge for nuclear theories, such as the intricate behavior of charge radii along the Ca isotopic chain [6] and the reduction in odd-even staggering of charge radii of exotic copper isotopes approaching $N = 50$ shell gap [7]. Therefore, the study of nuclear charge radius becomes a hot topic in nuclear physics during past decades.

Nuclear charge radius can be measured by electronic scattering experiments [8,9] and muonic spectra [10,11], or extracted from the optical [12] and K_α x-ray [13] isotope shifts. The optical isotope shifts can be used to determine charge radii of weakly produced exotic isotopes, so the charge radius measurements have been extended to the regions far from the β-stability line for some isotopic chains with the development of laser spectroscopy [14,15]. The charge radii of about 200 nuclides measured by laser spectroscopy experiment were compiled in Ref. [16], and about 900 nuclear charge radii were summarized and evaluated by combined analysis of the experimental data from various methods in Ref. [17].

The liquid drop model [18,19] treats a nucleus as a uniform liquid drop with a sharp surface, in which the charge radius can be described with a phenomenological formula. Since its introduction various phenomenological formulas have been proposed to improve the theoretical description of nuclear charge radius [20–24]. With the development of computer techniques and computational methods, it is possible to predict nuclear charge radii with *ab initio* method [7,25]. It can well describe the local features of the charge radii, whereas there are systematic deviations to the experimental absolute charge radii [7]. In addition, it is very difficult or even impossible to make systematic calculations for heavy nuclei with *ab initio* method. Density functional theory (DFT) [26] is another method to describe nuclear charge radii, which can well reproduce the experimental isotope shift including the conspicuous kink around the magic number [27], within the nonrelativistic [28–33] and the relativistic [34,35] frameworks. In contrast to the nonrelativistic model, the relativistic model [36–39] has some attractive advantages including automatic inclusion of nucleonic spin degree of freedom, natural description of the nuclear spin-orbit coupling with an empirical strength, natural explanation of the pseudospin symmetry in the nucleon spectrum [40–42], and the spin symmetry in antinucleon spectrum [42,43]. The relativistic model has been successfully applied to describe various nuclear properties, such as nuclear masses [44–46], half-lives [47–49], fission properties [50–52], nuclear rotations [53,54], low-lying spectrum [55,56], and spin-isospin resonances [57–59]. Therefore, it is appropriate to systematically study nuclear charge radii with the relativistic DFT.

*zmniu@ahu.edu.cn

The pairing correlation and continuum effects are essential to investigate many nuclear properties [60], and the relativistic continuum Hartree-Bogoliubov (RCHB) theory has considered these effects via the Bogoliubov transformation in the coordinate representation [61,62], so the RCHB theory has been applied to describe ground-state properties of spherical nuclei. The RCHB theory has been applied to describing ground-state properties of spherical nuclei, such as the interpretation of halo phenomena [61] and predict giant halo phenomena [63,64]. It has been also employed to construct nuclear mass table and the inclusion of continuum effects largely extends the existing nuclear landscapes predicted with other methods [65], while its predictions have obvious deviations to experimental masses for many deformed nuclei. By including the deformation degree of freedom, the deformed relativistic Hartree-Bogoliubov theory in continuum (DRHBc) has been developed based on a Dirac Woods-Saxon basis [66–68]. The DRHBc theory provides a unified description for all nuclei in the nuclear chart, even including those open-shell deformed nuclei near drip line, since it simultaneously contains the pairing correlation, deformation, and continuum effects.

Due to the advantages of the DRHBc theory in describing nuclear ground-state properties, it has been employed to study many nuclear phenomena successfully, such as deformed halo [66,67,69–75], particles in the classically forbidden regions [76], shape coexistence [77,78], deformation effects on the location of neutron drip line [79], and the peninsulas of stability beyond the two-neutron drip line [80–82]. Another important application of DRHBc theory is the construction of nuclear mass table with the PC-PK1 effective interaction [83]. The strategy and techniques for the nuclear mass table by the DRHBc theory are presented for even-even nuclei in Ref. [84] and odd-mass nuclei in Ref. [85]. The mass table for even-even nuclei has been summarized in Ref. [44], whose root-mean-square (rms) deviation of nuclear masses to the experimental data is about 1.5 MeV by including the rotational correction energies in the cranking approximation, providing one of the best microscopic descriptions for nuclear masses. However, the cranking approximation used to obtain the rotational correction energy in the present DRHBc calculations is not suitable for (near) spherical nuclei (quadrupole deformation $\beta_2 \leqslant 0.05$). Therefore, its description of nuclear mass for (near) spherical nuclei is generally worse than that for deformed nuclei [86], and nonphysical kinks of two-neutron separation energies S_{2n} are found when the nuclei change from (near) spherical to deformed shapes [87]. It is found that the beyond-mean-field dynamical correlation energies (DCEs) can improve the description of both deformed and (near) spherical nuclei by using the five-dimensional collective Hamiltonian (5DCH) [88–92] or generator coordinate method (GCM) methods [93]. Systematical calculations of DCEs have been performed based on the axially deformed relativistic mean-field plus Bardeen-Cooper-Schrieffer (BCS) (RMF+BCS) [94] and triaxial relativistic Hartree-Bogoliubov (RHB) theories in the harmonic oscillator basis [95]. Compared with the harmonic oscillator basis, the Woods-Saxon basis is more suitable to describe the exotic nuclei and hence to perform large-scale calculations since it has a more realistic asymptotic behavior. Recently, the DRHBc theory has been extended to go beyond mean-field framework by performing a two-dimensional collective Hamiltonian (2DCH) [87]. It is found that DCEs with 2DCH method can significantly improve the description of nuclear masses for the (near) spherical nuclei by taking Se, Nd, and Th isotopes as examples, and reduce the rms deviations of S_{2n} by 17% [87].

Nuclear deformation plays an important role in reliably describing many nuclear properties, such as nuclear masses mentioned above and charge radii. It has been found that the drastic changes in the charge radii of Sr and Zr isotopes at $N = 60$ are related to the rapid changing in nuclear shapes [96–98]. The shape evolution and shape coexistence at $N \approx 60$ have attracted wide attention from both theoretical and experimental sides, e.g., the related experimental measurements for ^{72}Kr [99], Sr isotopes [100–102], and ^{98}Zr [103], and theoretical studies for Kr isotopes [104], Kr, Sr, and Zr isotopes [2], Sr isotopes [105], Sr and Zr isotopes [106,107], and Zr isotopes [108–112]. These studies have shown that there are complicated shape evolution and rich structure information in Kr and Sr isotopes. For better treating the weakly deformed nuclei and large shape fluctuations related to a very soft potential energy curve (PEC) around the global minima in Kr and Sr isotopes, we would employ the 2DCH method to consider the beyond-mean-field dynamical correlation effects based on the calculations of DRHBc theory. The results of Kr and Sr isotopes with DRHBc+2DCH model are presented in Sec. III, and special attention is focused on nuclear charge radii and shape evolution. A brief introduction of DRHBc+2DCH model is given in Sec. II. The summary and perspectives are presented in Sec. IV.

II. THEORETICAL FRAMEWORK

The DRHBc theory provides a unified and self-consistent treatment of the mean field and the pairing correlation, which can include continuum effects without introducing nonphysical contributions and describe the exotic nuclei properly in the Dirac Woods-Saxon basis [113,114]. The details of DRHBc theory can be found in Refs. [66,67,84], so we only give a brief introduction of DRHBc theory here.

The relativistic Hartree-Bogoliubov equations [115] in DRHBc theory,

$$\begin{pmatrix} h_D - \lambda_\tau & \Delta \\ -\Delta^* & -h_D^* + \lambda_\tau \end{pmatrix} \begin{pmatrix} U_k \\ V_k \end{pmatrix} = E_k \begin{pmatrix} U_k \\ V_k \end{pmatrix}, \quad (1)$$

are solved in the Dirac Woods-Saxon basis [113,114]. E_k is the quasiparticle energy, $(U_k, V_k)^\top$ is the quasiparticle wave function, and λ_τ is the Fermi energy for neutron or proton ($\tau = n, p$). The Dirac Hamiltonian h_D is

$$h_D(\boldsymbol{r}) = \boldsymbol{\alpha} \cdot \boldsymbol{p} + V(\boldsymbol{r}) + \beta[M + S(\boldsymbol{r})], \quad (2)$$

where M is the neutron (proton) mass, and $S(\boldsymbol{r})$ and $V(\boldsymbol{r})$ are the scalar and vector potentials, respectively. In this work, the potentials $S(\boldsymbol{r})$ and $V(\boldsymbol{r})$ are derived from the Lagrangian with the effective point-coupling interaction PC-PK1 [83]. The pairing potential Δ is

$$\Delta(\boldsymbol{r}_1, \boldsymbol{r}_2) = V^{pp}(\boldsymbol{r}_1, \boldsymbol{r}_2)\kappa(\boldsymbol{r}_1, \boldsymbol{r}_2), \quad (3)$$

where κ is the pairing tensor. V^{pp} is the pairing force and in this work we use a density-dependent zero-range pairing force

$$V^{pp}(\boldsymbol{r}_1, \boldsymbol{r}_2) = V_0 \frac{1}{2}(1 - P^\sigma)\delta(\boldsymbol{r}_1 - \boldsymbol{r}_2)\left(1 - \frac{\rho(\boldsymbol{r}_1)}{\rho_{\text{sat}}}\right). \quad (4)$$

Here, V_0 and ρ_{sat} are the pairing strength and the saturation density of nuclear matter, respectively. $(1 - P^\sigma)/2$ is the projector for the spin $S = 0$ component in the pairing channel. For axially deformed nuclei, the potentials are expanded with the Legendre polynomials in the DRHBc theory

$$f(\boldsymbol{r}) = \sum_\lambda f_\lambda(r)P_\lambda(\cos\theta), \quad \lambda = 0, 2, 4, \ldots, \lambda_{\max}. \quad (5)$$

Because of the spatial reflection symmetry, λ is restricted to be even numbers. The numerical details of DRHBc calculation are the same as suggested in Ref. [84]. Specifically, the Legendre extension truncation in Eq. (5) is chosen as $\lambda_{\max} = 6$, the pairing strength and saturation density in Eq. (4) are set as $V_0 = -325$ MeV fm^3 and $\rho_{\text{sat}} = 0.152$ fm^{-3}, and a cutoff energy of 100 MeV is used for the pairing window in the quasiparticle space.

Similar to Refs. [82,84], the charge radius R_c is calculated with

$$R_c = \sqrt{R_{p,\text{rms}}^2 + 0.64 \text{ fm}^2}, \quad (6)$$

which ignores the small correction due to the center of mass motion and the charge distributions in proton and neutron [116,117]. The root-mean-square (rms) radius of proton $R_{p,\text{rms}}$ can be obtained with

$$R_{p,\text{rms}}^2 = \int d^3\boldsymbol{r}[r^2\rho_p(\boldsymbol{r})]/Z, \quad (7)$$

where ρ_p is the vector density of the proton.

To include the collective dynamical correlations, the 2DCH method is employed to go beyond mean-field approximation, whose collective parameters are determined from the constrained DRHBc calculations [87]. The 2DCH collective Hamiltonian is

$$\hat{H}_{\text{coll}} = \hat{T}_{\text{vib}} + \hat{T}_{\text{rot}} + V_{\text{coll}}$$
$$= -\frac{\hbar^2}{2}\frac{1}{\sqrt{\mathscr{I}B_{\beta\beta}}}\frac{\partial}{\partial\beta}\sqrt{\frac{\mathscr{I}}{B_{\beta\beta}}}\frac{\partial}{\partial\beta} + \frac{\hat{J}^2}{2\mathscr{I}} + V_{\text{coll}}, \quad (8)$$

where $\hat{T}_{\text{vib}}$ and $\hat{T}_{\text{rot}}$ are the vibrational and rotational kinetic energy terms, respectively. V_{coll} is the collective potential, which is calculated from the DRHBc total energy by subtracting the rotational correction energy E_{rot} and the vibrational correction energy E_{vib}. $B_{\beta\beta}$ is the collective mass, which is calculated in the cranking approximation [118]. $\hat{J}$ is the total angular momentum in the intrinsic frame and $\mathscr{I}$ is the moment of inertia, which is calculated by the Inglis-Belyaev inertial function [119,120]. One can obtain the beyond-mean-field ground-state energy $E(0_1^+)$ by diagonalizing the 2DCH Hamiltonian $\hat{H}_{\text{coll}}$ in Eq. (8). The dynamical correlation energy is then calculated with the difference between the global minimum of the total energy curve and $E(0_1^+)$, i.e., DCE $= E_{\text{tot}}^{\min} - E(0_1^+)$.

The continuum effects play an important role in studying the properties of exotic nuclei, especially for nuclei near the drip lines. Therefore, a nuclear model with continuum effects is necessary to perform large-scale calculations for nuclei on the nuclear chart. By further including the 2DCH corrections, the DRHBc model can better describe nuclear properties with low computational limitation, thus providing an effective tool to systematically study nuclear properties. However, it should be noted that the present calculations are limited to the axial degree of freedom and the results may be affected for some triaxially deformed nuclei.

III. RESULTS AND DISCUSSION

The binding energy and two-neutron separation energy are first employed to show the predictive powers of DRHBc and DRHBc+2DCH models, whose results are presented in Figs. 1 and 2, respectively. From Fig. 1, it is clear that the DRHBc generally underestimates nuclear binding energies, whose rms deviation with respective to the experimental data [121] is 3.0 MeV for Kr and Sr isotopes. It has been found that the rotational correction energies E_{rot} should be included properly in the DRHBc calculations with PC-PK1, which are obtained in the cranking approximation here as in Ref. [84]. By including the E_{rot}, the description of deformed nuclei is remarkably improved, and the rms deviation is reduced to 1.8 MeV. However, the E_{rot} is set to be zero for (near) spherical nuclei ($\beta_2 \leqslant 0.05$), since the cranking approximation is not suitable and nonphysical results would be obtained for them. Based on the 2DCH method, the obtained DCEs not only improve the description of deformed nuclei but also improve the description of (near) spherical nuclei ^{76,78,86}Kr and ^{80,82,84,86,88}Sr close to the neutron (sub)shell, further reducing the rms deviation to 1.2 MeV. Therefore, the DCEs are essential for describing nuclei with different deformations, including (near) spherical nuclei. However, the binding energies of some nuclei are still underestimated even with the 2DCH corrections, e.g., ^{88,90}Kr and ^{90,92,94}Sr. The inclusion of triaxial degrees of freedom can help to improve these deviations. Compared with the present 2DCH calculations, the 5DCH calculations in Ref. [95] can further reduce the rms of binding energies of Kr and Sr isotopes by about 0.1 MeV. This small rms improvement might suggest that the triaxial degree of freedom does not influence seriously.

The two-neutron separation energy S_{2n} contains detailed information about the nuclear structure, such as shell structure and shape transition, whose results are shown in Fig. 2 for Kr and Sr isotopes. The DRHBc, DRHBc with E_{rot}, and DRHBc+2DCH models all reproduce the shell structure at the magic number $N = 50$, but the shell gap of DRHBc is too large, which can be improved by adding the E_{rot} in cranking approximation or the DCEs with 2DCH method. Moreover, conspicuous non-physical kinks of S_{2n} are found around $N = 40$ for both Kr and Sr isotopes when the E_{rot} is added to DRHBc calculations. It is found that these kinks originate from abrupt changes of deformations, e.g., shape changes from largely deformed nuclei ^{74}Kr and ^{78}Sr to spherical nuclei ^{76}Kr and ^{80}Sr (refer to Fig. 4 for the deformations of Kr and Sr isotopes). There are about 3 MeV for the E_{rot} of largely deformed nuclei, while they are zero for (near) spherical nuclei, so abrupt changes of deformations induce
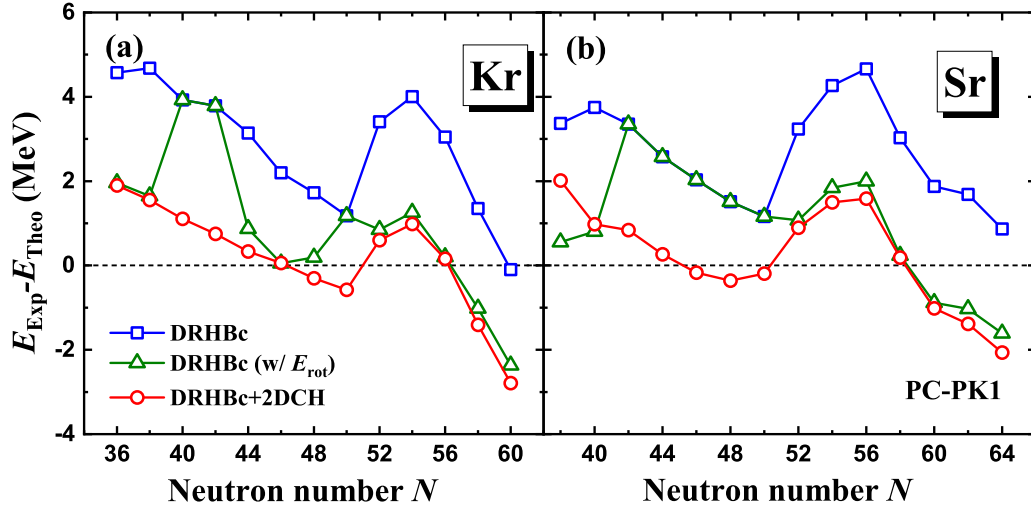
FIG. 1. Differences between the experimental binding energies [121] and the theoretical results for Kr (a) and Sr (b) isotopes. The DRHBc results, DRHBc results with E_{rot}, and DRHBc+2DCH results are shown by open squares, triangles, and circles, respectively.

the abrupt changes of E_{rot} and hence induce the conspicuous kinks of S_{2n}. By considering the beyond-mean-field dynamical correlation with 2DCH method, the changes of deformations are remarkably weakened and there are nonzero DCEs for both deformed and spherical nuclei, so the kinks of S_{2n} in both Kr and Sr isotopes are well eliminated and hence the S_{2n} predicted by DRHBc+2DCH are more consistent with the experimental data [122]. And the rms deviation of S_{2n} are 1.01 MeV, 1.16 MeV, and 0.77 MeV for the DRHBc, the DRHBc with E_{rot}, and DRHBc+2DCH theories, respectively. Therefore, the inclusion of dynamical correlations with 2DCH makes the DRHBc predictions more reliable, and we will employ the DRHBc+2DCH model to study the evolution of deformations and charge radii of Kr and Sr isotopes in the following.

The two-neutron separation energy can also be used to determine the neutron drip line. The neutron drip-line nuclei for Kr and Sr isotopes predicted by the DRHBc+2DCH

are ^{132}Kr and ^{142}Sr. The drip-line nuclei predicted by the RHB in the harmonic oscillator basis are ^{130,120,118,118}Kr and ^{138,126,120,120}Sr for NL3*, DD-ME2, DD-MEδ, and DD-PC1, respectively [123]. Clearly, the inclusion of the continuum can extend the neutron drip line to the more neutron-rich side. Compared to the drip-line nuclei ^{136}Kr and ^{148}Sr predicted by the spherical RCHB [65], the inclusion of deformation would also affect the position of the neutron drip line. If only E_{rot} are considered in the DRHBc calculations, the conspicuous nonphysical kinks are found when $N > 60$ regions for both Kr and Sr isotopes, such as around $N = 68, 80, 84, 92$ for Kr isotopes. This kind of kink induces ^{128}Kr to be unbound, and hence ^{126}Kr becomes the neutron drip line, showing the importance of DCE effects in the determination of the neutron drip line. The above discussions show that the simultaneous consideration of the deformation, continuum, and DCE effects is important for the determination of the drip line, which can be achieved in the DRHBc+2DCH theory.
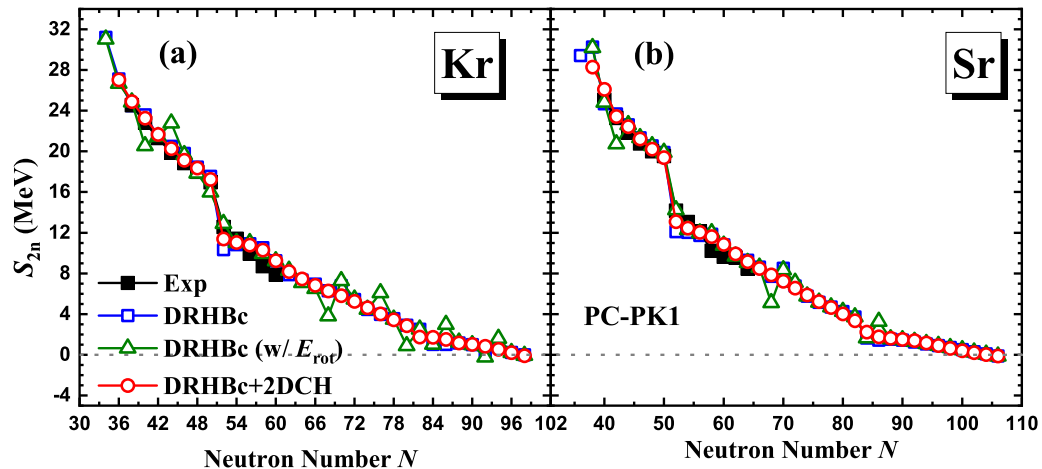

FIG. 2. Comparison of S_{2n} between experimental data [121] (filled squares) and theoretical results for Kr (a) and Sr (b) isotopes. The DRHBc results, DRHBc results with E_{rot}, and DRHBc+2DCH results are shown by open squares, triangles, and circles, respectively.
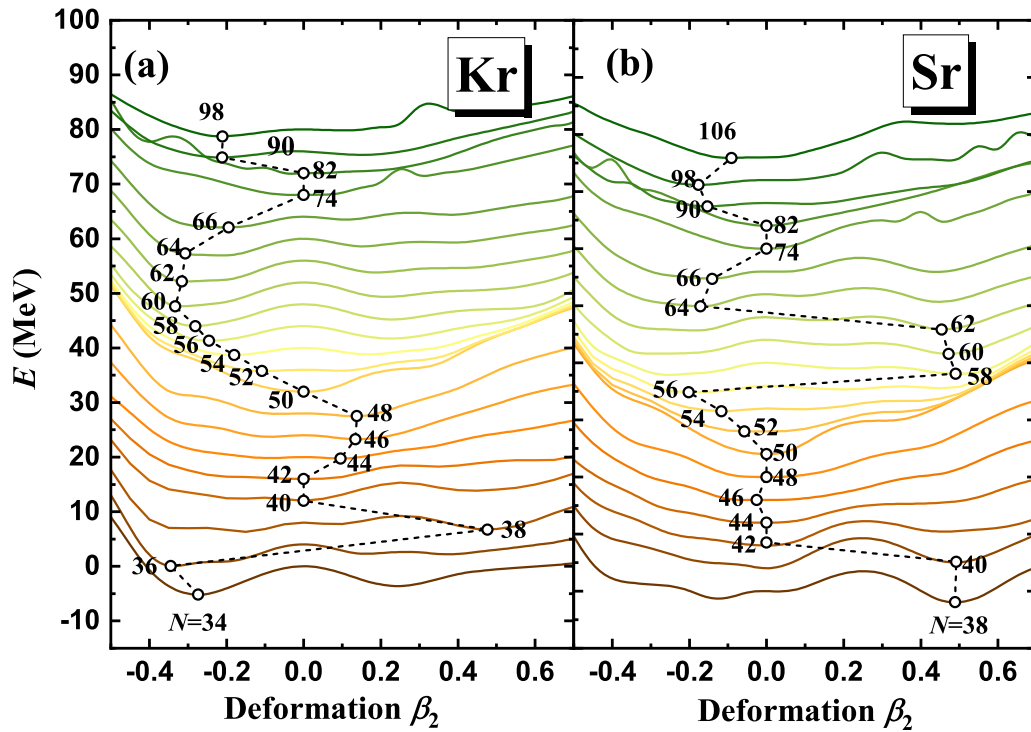
FIG. 3. Evolution of the PECs for Kr (a) and Sr (b) isotopes from the constrained DRHBc calculations. For displaying the data clearly, the PECs of the lightest isotopes ^{70}Kr and ^{76}Sr are renormalized to their potential energies at $\beta_2 = 0$, and other PECs for each isotope are shifted upward by 4 MeV compared to the previous one.
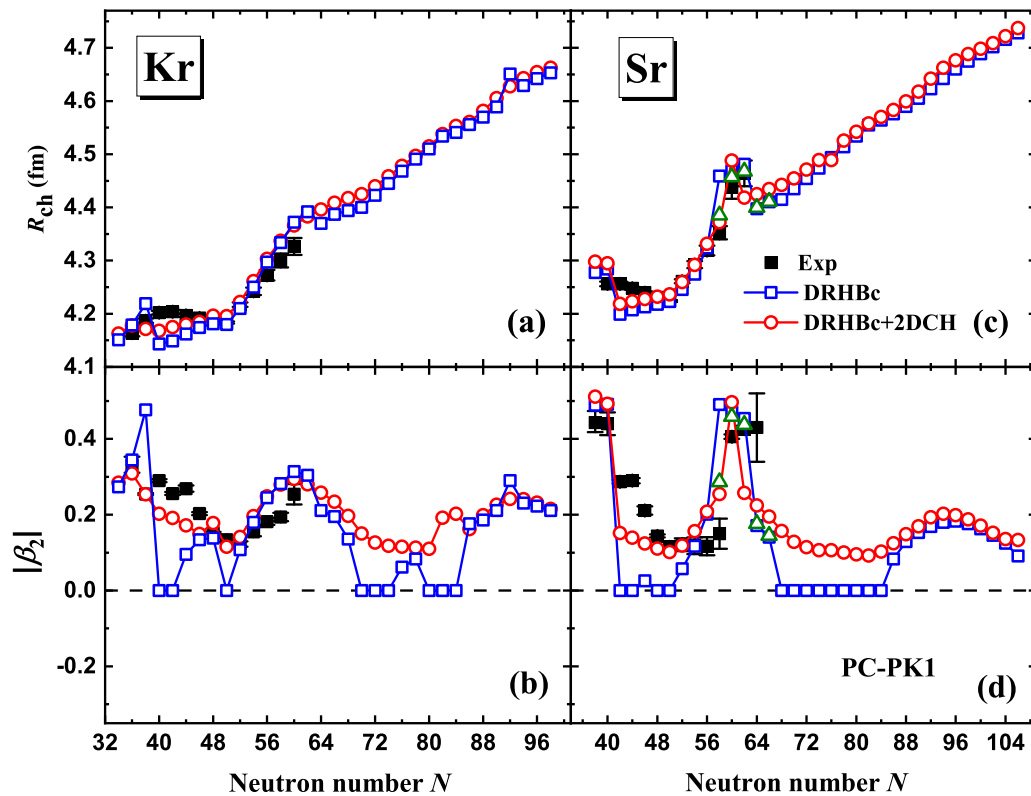

FIG. 4. Charge radii and deformations for Kr and Sr isotopes. The results from the DRHBc+2DCH and DRHBc calculations are denoted with open circles and open squares, respectively. The green triangles (c) and (d) represent the new DRHBc+2DCH calculations, while the pairing strength is reduced by multiplying a factor of 0.8. The corresponding experimental data [17,122] are shown with filled squares for comparison.

Rich structure and shape coexistence phenomena have been widely noticed in Kr and Sr isotopes [2,97–102,104–106]. The potential energy curves (PECs) are very crucial to study nuclear structure and shape evolution, which are shown in Fig. 3(a) and 3(b) for Kr and Sr isotopes, respectively. The global minima of PECs are denoted by open circles in Fig. 3. It is known that the nucleus with a magic number is generally spherical, e.g., ^{86}Kr at neutron magic number $N = 50$. When the neutron number deviates (decreases or increases) from magic number $N = 50$, soft PECs are found for $^{76-84,88}$Kr ($N = 40-48, 52$). When the neutron number decreases to $N = 38$, a very complex structure shows up for ^{74}Kr. It has a prolate global minimum and a soft potential energy curve around the oblate minima, whose energy difference between two minima is only 0.041 MeV. ^{72}Kr ($N = 36$) has an oblate global minimum and a soft potential around the prolate minima, while the energy difference between two minima is 2.356 MeV. Moving along the chain in neutron-deficient direction, two remarkable minima are found for ^{70}Kr ($N = 34$), one is oblate ground states and the other is prolate local minimum, and the energy difference between the two minima is 1.566 MeV. With the increase of neutron number, two minima at oblate and prolate shapes are also found from ^{90}Kr ($N = 54$), whose energy differences are 0.078, 0.447, 1.271, 3.352, and 2.516 MeV for $^{90-98}$Kr, respectively. Therefore, ^{74,90,92}Kr are possible candidates for shape coexistence in the DRHBc calculations, since their energy differences ΔE between two minima are very small (criterion of $\Delta E \lesssim 1$ MeV as in Refs. [77,78]). Moving further towards the neutron-rich side, the PECs have (near) spherical minima for the nuclei around the next magic number $N = 82$, others have prolate or oblate minima. Similar shape evolution is also found for Sr isotopes, e.g., ^{88}Sr ($N = 50$) is spherical and $^{80-86,90,92}$Sr ($N = 42-48, 52, 54$) have soft potentials. Moreover, there are two minima at oblate and prolate shapes for $^{76,78,94-104}$Sr ($N = 38, 40, 56-66$), and the energy differences between their oblate and prolate minima are all very small, which are 1.008, 0.267, 0.355, 0.137, 0.348, 0.205, 0.450, 0.849 MeV, respectively. These small energy differences between two minima imply that they are possible candidates for shape coexistence. For the nuclei around the next magic number $N = 82$, i.e., the nuclei with $N = 70-84$, their PECs all have spherical minima. Moving further towards the neutron-rich side for Sr isotopes, the deformations of their ground states are stabilized in the oblate shape.

In comparison with the triaxial RHB theory [95], we found that there is no triaxial deformation in the ground state for the Kr and Sr isotopes. This triaxial RHB theory employed the PC-PK1 density functional to systematically calculate the nuclear landscape and accounted for DCEs through the 5DCH method. Many ground state properties calculated within the 2DCH model are in good agreement with the data, for example, the experimental binding energy results shown in Fig. 1. As mentioned above, the small reduction of rms of binding energies from 2DCH to 5DCH calculations might suggest that the triaxial degree of freedom does not influence seriously. However, even though no energy minimum is found at triaxiality, the triaxial degree of freedom may still influence the results of some nuclei with double minima. By

carefully checking the triaxial calculations in Ref. [95], we found that the nuclei just above $N = 50$ have a clear path connecting them in the β-γ plane with relatively low energies, for which an admixture of the γ-deformed configuration may be important, such as ^{88,90}Kr and ^{90,92,94}Sr. A systematic search for triaxial ground-state nuclear shapes in Kr and Sr isotopes has also been studied within a relativistic DFT using DD-PC1 and NL3* parameter sets, which predicted that there are the triaxial deformations in the ground states of ^{92,94}Sr [2]. This further suggests that the triaxial degree of freedom may be important for the nuclei just above $N = 50$. Therefore, it should be noted that the present results of these nuclei may be affected if one includes the triaxial degree of freedom.

The deformations of DRHBc theory can be obtained from the global minima of PECs, which are shown in Fig. 4 for Kr and Sr isotopes together with their charge radii. As discussed in Fig. 3, soft potentials around the global minima are found for nuclei with neutron number around magic number $N = 50$. The shape predictions for these nuclei are very challenging for the mean-field model. The 2DCH method can well deal with the large shape fluctuations characterized by soft potentials, and the deformations in the 2DCH method can be calculated as the expectation values of β_2 in the ground state 0_1^+ [87]. From Fig. 4(b) and 4(d), it is clear that the DRHBc+2DCH gives nonzero deformations for all Kr and Sr isotopes with $N = 40-52$ due to the shape fluctuations. The calculated deformations with the DRHBc+2DCH better agree with the experimental deformation data extracted from measured $B(E2)$ [122]. For neutron-rich Kr and Sr isotopes around the next magic number $N = 82$, the DRHBc+2DCH also gives nonzero deformations as for the nuclei around $N = 50$, so the deformation evolution predicted by the DRHBc+2DCH is much smoother than that predicted by the DRHBc. The abrupt shape changes between deformed nuclei and spherical nuclei can lead to the abrupt changes of $E_{\rm rot}$, which then induce the nonphysical kinks of S_{2n} shown in Fig. 2. Therefore, the DECs from 2DCH are important for our understanding of nuclear ground-state properties.

For ^{74}Kr and ^{96}Sr, possible candidates for shape coexistence with energy differences between two minima as 0.041 and 0.137 MeV, the DRHBc predicts very large prolate deformations $|\beta_2| > 0.4$, while the DRHBc+2DCH predicts oblate ground states with moderate deformations $|\beta_2| \approx 0.25$, which agree well with the experimental values. This implies the importance of dynamical correlations by the 2DCH in describing some nuclei with shape coexistence. Therefore, the DRHBc+2DCH can also improve the description of deformation for the deformed nuclei with $\beta_2 \gtrsim 0.2$. However, the DRHBc+2DCH predicts an oblate ground state for ^{100}Sr with $|\beta_2| = 0.258$, which is much smaller than its experimental value of 0.426. It has been found the 2DCH calculations are quite sensitive to the pairing correlations [87], so we further reduce the pairing strength by multiplying a factor of 0.8 (from $V_0 = -325$ to -260 MeV fm^3) to make DRHBc+2DCH calculations and the new results are shown by triangles in Fig. 4(c) and 4(d) for $^{96-104}$Sr. For ^{100}Sr, the ground state becomes prolate shape with $|\beta_2| = 0.437$ from oblate shape with $|\beta_2| = 0.258$.
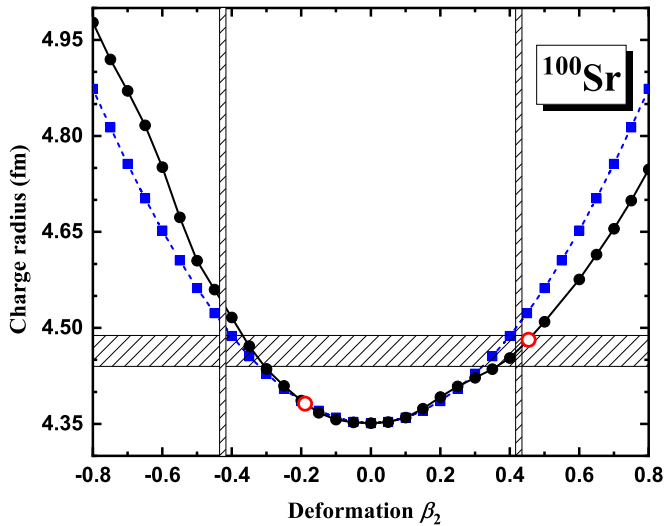
FIG. 5. Charge radius as a function of deformation for ^{100}Sr. The filled and open circles denote the constrained results and the minima in unconstrained calculations predicted by the DRHBc model. The dependence between the charge radius and the deformation from a empirical formula [124] is shown with the squares for comparison. Shadows represent experimental charge radius [17] and deformation [122] with uncertainties.

FIG. 6. Wave function of ^{100}Sr in the 2DCH model.

It is also found that the 5DCH calculations based on RMF+BCS [98,106] well reproduce the experimental charge radii of Sr isotopes including ^{100}Sr, which may imply the triaxial degree of freedom is also important for some Sr isotopes. As can be seen in Fig. 3, some nuclei have two minima, and the deformations may change when considering the triaxial degree of freedom, especially for the nuclei just above $N = 50$. Nuclear charge radii are sensitive to nuclear deformations, so the improvement of nuclear deformation in DRHBc+2DCH model induces the improvement of nuclear charge radii. For example, the inclusion of dynamical correlations with 2DCH method based on the DRHBc calculations improves the underestimation of charge radii for (near) spherical Kr and Sr isotopes and smooths the non-physical kink of charge radius at $N = 38$ and 92 for Kr isotopes. Therefore, the DRHBc+2DCH model generally better reproduces the experimental charge radii than DRHBc model for both (near) spherical and deformed nuclei.

To further study the dependence of charge radius on deformation, nuclear charge radii are shown in Fig. 5 as a function of deformation by taking ^{100}Sr as an example. The dependence between the charge radius and the deformation from a well-known empirical formula [124] is also shown for comparison, i.e., $R_{ch}^2 = R_{ch0}^2[1 + 5\beta_2^2/(4\pi)]$. The R_{ch0} represents the charge radius of the corresponding spherical nucleus. This empirical formula is derived by assuming a phenomenological charge density distribution, while the present DRHBc theory can make self-consistent calculations, which generally better describes nuclear density distributions. From the constrained calculations with the DRHBc theory, it is clear that the charge radius takes the smallest value when the nucleus is spherical and it increases with the increase of deformation
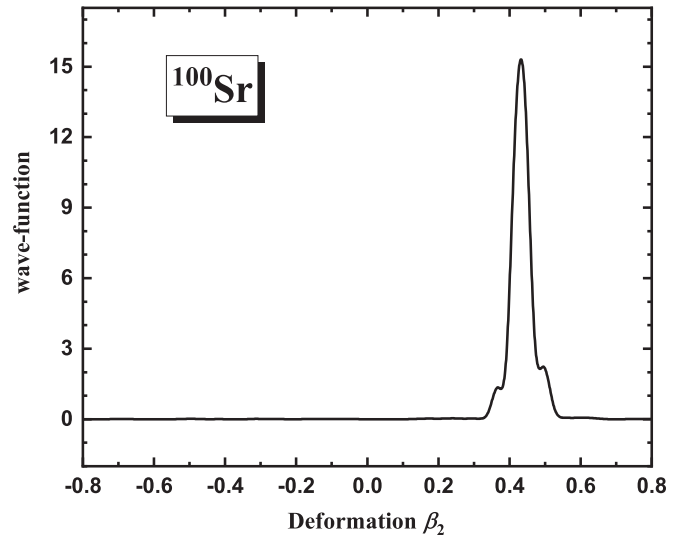
in both oblate and prolate sides. However, the charge radius increases more rapidly along the oblate direction, so the same charge radius would correspond to different deformations in the oblate and prolate regions. When the charge radius and the absolute value of deformation $|\beta_2|$ are known, one can determine whether a nucleus is oblate or prolate when the deformation $|\beta_2| \gtrsim 0.3$. The experimental deformation data are extracted from the measured $B(E2)$ by using the relation $\beta_2 = 4\pi e\sqrt{B(E2)}/(3ZR_0^2)$ with $R_0 = 1.2A^{1/3}$ fm [122]. Clearly, there are only positive β_2 for experimental deformations, which are in fact the magnitude of β_2, i.e., $|\beta_2|$. Therefore, it is believed that the $B(E2)$ does not depend on the sign of β_2, which is valid for strongly deformed nuclei. The experimental data of other nuclear properties are then necessary to determine the sign of β_2. We have found that the charge radii are very sensitive to the sign of β_2 for the strongly deformed nuclei with $|\beta_2| \gtrsim 0.3$. One can then combine the experimental $|\beta_2|$ extracted from measured $B(E2)$ and the experimental charge radii to determine the sign of β_2 for the nuclei with $|\beta_2| \gtrsim 0.3$.

Taking ^{100}Sr as an example, its experimental charge radius R_{ch} and deformation β_2 with uncertainties are shown by the horizontal and vertical shadows in Fig. 5, respectively. Clearly, the experimental charge radius and deformation can be achieved simultaneously only when the nucleus takes a prolate shape. The DRHBc also predict a prolate minimum at this region, which agree well with the experimental charge radius and deformation. Furthermore, it can be seen from Fig. 4 that the DRHBc+2DCH model also predicts a prolate shape with $\beta_2 = 0.437$ when it can reproduce the experimental charge radius of ^{100}Sr. The corresponding wave function in the 2DCH model is shown in Fig. 6. It is clear that the prolate deformation with $\beta_2 \approx 0.45$ is the dominant component, which further testifies that the correlation between charge radius and deformation can help to determine the oblate or prolate shape of a nucleus.

Figure 7 presents the charge radii from the DRHBc calculations for Kr and Sr isotopes, whose deformations are
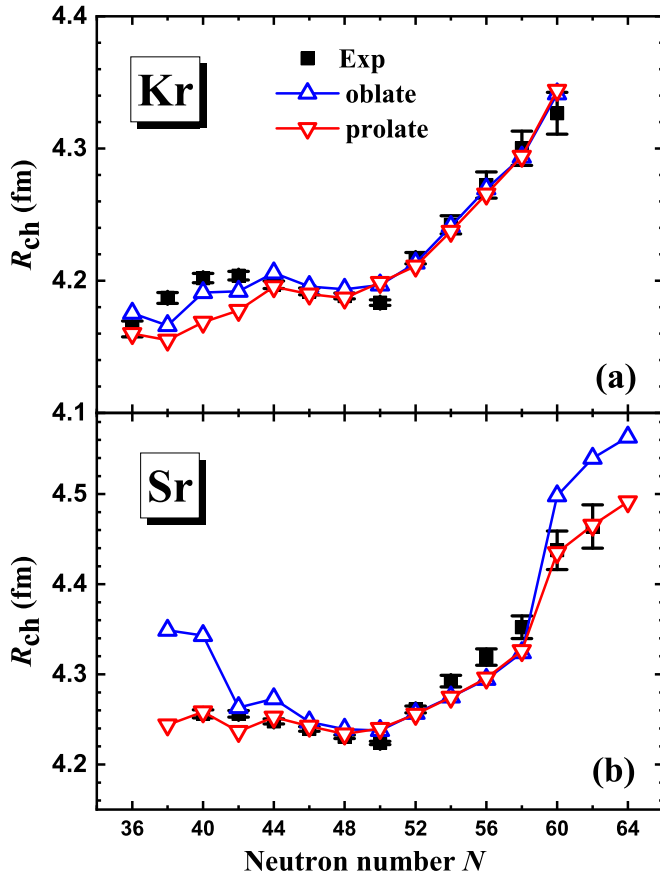
FIG. 7. Charge radii from the constrained DRHBc calculations for Kr (a) and Sr (b) isotopes. The deformations in DRHBc calculations are constrained to the experimental values [122] in the prolate (open inverted triangles) and oblate (open triangles) regions. The experimental charge radii [17] are shown with filled squares for comparison.

so the inclusion of triaxial degree of freedom may affect our results.

IV. SUMMARY AND PERSPECTIVES

The DRHBc is employed to study the ground-state properties of Sr and Kr isotopes, including the binding energies, two-neutron separation energies, deformations, and charge radii. Based on the DRHBc calculations, the beyond-mean-field dynamical correlation effects are considered with 2DCH method. It is found that the DCEs are essential for describing nuclei with different deformations, including (near) spherical nuclei, and thus reducing the rms deviation of binding energies from 3.2 MeV to 1.2 MeV. The DRHBc+2DCH model reduces the shell gap of $N = 50$ and eliminates the nonphysical kinks of S_{2n} in DRHBc calculations, hence better describes experimental S_{2n}. Based on the constrained DRHBc calculations, it is found that Kr and Sr isotopes (^{86}Kr and ^{88}Sr) with $N = 50$ are spherical, while the nuclei just away from $N = 50$ generally have soft PECs. Further moving along the isotopic chains in both neutron-rich and neutron-deficient directions, there are generally two minima at oblate and prolate shapes for nuclear PECs, where possible candidates for shape coexistence are found, e.g., ^{74,90,92}Kr and $^{76,78,94-104}$Sr. The dynamical correlations are found to be crucial to describe deformations of nuclei with soft PECs or shape coexistence. Therefore, the DRHBc+2DCH gives nonzero deformations for the (near) spherical nuclei in DRHBc theory due to the shape fluctuations, and thus better reproduces the experimental deformations extracted from measured $B(E2)$. The improvement of nuclear deformation in DRHBc+2DCH model induces the improvement of nuclear charge radii. However, one also needs to be aware that the 2DCH calculations are quite sensitive to the pairing correlations. Finally, it is found that the constrained DRHBc calculations are helpful to distinguish the oblate or prolate shape for the nuclei with deformation $|\beta_2| \gtrsim 0.3$ by combining with the experimental charge radii and absolute values of deformations. Based on the present calculations, $^{74-78}$Kr and ^{80}Sr are more likely to be oblate, while ^{78,82,98,100}Sr are more likely to be prolate. In Ref. [95], it is found that the ground states of Kr and Sr isotopes considered here are not triaxially deformed with the 5DCH method based on the RHB theory in harmonic oscillator basis and the effective interaction PC-PK1. However, it would be interesting to extend the DRHBc theory from the present axial deformation to include triaxial degree of freedom and consider the dynamical correlation effects with the 5DCH method in future works, which would be helpful to confirm our conclusions in this work.

constrained to their experimental values in the prolate and oblate regions. Clearly, at least one charge radius from the constrained DRHBc calculation can reproduce the experimental value. Combining Figs. 4 and 7, it is found that the charge radii from the constrained DRHBc calculations of some nuclei are close to the experimental values in both prolate and oblate regions, such as $^{82-96}$Kr ($N = 46-60$) and $^{84-96}$Sr ($N = 46-58$), corresponding to nuclei with relatively weak deformation $|\beta_2| \lesssim 0.25$. For the relatively largely deformed nuclei, especially for $|\beta_2| \gtrsim 0.3$, the charge radii from the constrained DRHBc calculations are clearly different from each other, and only one constrained result can reproduce the experimental charge radii, so that one can distinguish the nuclear deformation in the prolate or oblate region. The present DRHBc calculations support that $^{74-78}$Kr ($N = 38-42$) and ^{80}Sr ($N = 42$) are more likely to be oblate, while ^{78,82,98,100}Sr ($N = 40, 44, 60, 62$) are more likely to be prolate. Therefore, the constrained DRHBc calculations can be used to distinguish the oblate or prolate shape for the largely deformed nuclei with $|\beta_2| \gtrsim 0.3$ by combining the experimental charge radius and absolute values of deformation. It should be noted that the present work is limited in the axial degree of freedom,

[1] W. Nörtershäuser *et al.*, Phys. Rev. Lett. **102**, 062503 (2009).

[2] H. Abusara and S. Ahmad, Phys. Rev. C **96**, 064303 (2017).

[3] X. F. Yang *et al.*, Phys. Rev. Lett. **116**, 182502 (2016).

[4] K. Kreim *et al.*, Phys. Lett. B **731**, 97 (2014).

[5] C. Gorges *et al.*, Phys. Rev. Lett. **122**, 192502 (2019).

[6] R. F. Garcia Ruiz *et al.*, Nat. Phys. **12**, 594 (2016).

[7] R. P. de Groote *et al.*, Nat. Phys. **16**, 620 (2020).

[8] R. Hofstadter, H. R. Fechter, and J. A. McIntyre, Phys. Rev. **92**, 978 (1953).

[9] H. De Vries, C. W. De Jager, and C. De Vries, At. Data Nucl. Data Tables **36**, 495 (1987).

[10] R. Engfer, H. Schneuwly, J. L. Vuileumier, H. K. Walter, and A. Zehnder, At. Data Nucl. Data Tables **14**, 509 (1974).

[11] G. Fricke *et al.*, At. Data Nucl. Data Tables **60**, 177 (1995).

[12] H. J. Kluge, Hyperfine Interact. **196**, 295 (2010).

[13] E. Boehm and P. L. Lee, At. Data Nucl. Data Tables **14**, 605 (1974).

[14] A. Koszorús *et al.*, Nat. Phys. **17**, 439 (2021).

[15] T. D. Goodacre, A. V. Afanasjev, A. E. Barzakh, B. A. Marsh, S. Sels, P. Ring, H. Nakada, A. N. Andreyev, P. VanDuppen, N. A. Althubiti, B. Andel, D. Atanasov, J. Billowes, K. Blaum, T. E. Cocolios, J. G. Cubiss, G. J. Farooq-Smith, D. V. Fedorov, V. N. Fedosseev, K. T. Flanagan, L. P. Gaffney, L. Ghys, M. Huyse, S. Kreim, D. Lunney, K. M. Lynch, V. Manea, Y. MartinezPalenzuela, P. L. Molkanov, M. Rosenbusch, R. E. Rossel, S. Rothe, L. Schweikhard, M. D. Seliverstov, P. Spagnoletti, C. VanBeveren, M. Veinhard, E. Verstraelen, A. Welker, K. Wendt, F. Wienholtz, R. N. Wolf, A. Zadvornaya, and K. Zuber, Phys. Rev. Lett. **126**, 032502 (2021).

[16] T. Li, Y. Luo, and N. Wang, At. Data Nucl. Data Tables **140**, 101440 (2021).

[17] I. Angeli and K. P. Marinova, At. Data Nucl. Data Tables **99**, 69 (2013).

[18] C. F. V. Weizsäcker, Z. Phys. **96**, 431 (1935).

[19] H. A. Bethe and R. F. Bacher, Rev. Mod. Phys. **8**, 82 (1936).

[20] W. Myers and K. H. Schmidt, Nucl. Phys. A **410**, 61 (1983).

[21] B. Nerlo-Pomorska and K. Pomorski, Z. Phys. A **348**, 169 (1994).

[22] S. Q. Zhang, J. Meng, S. G. Zhou, and J. Y. Zeng, Eur. Phys. J. A **13**, 285 (2002).

[23] N. Wang and T. Li, Phys. Rev. C **88**, 011301(R) (2013).

[24] Z. Sheng, G. Fan, J. Qian, and J. Hu, Eur. Phys. J. A **51**, 40 (2015).

[25] A. Ekström, G. R. Jansen, K. A. Wendt, G. Hagen, T. Papenbrock, B. D. Carlsson, C. Forssén, M. Hjorth-Jensen, P. Navrátil, and W. Nazarewicz, Phys. Rev. C **91**, 051301(R) (2015).

[26] M. Bender, P. H. Heenen, and P. G. Reinhard, Rev. Mod. Phys. **75**, 121 (2003).

[27] T. Naito, T. Oishi, H. Sagawa, and Z. H. Wang, Phys. Rev. C **107**, 054307 (2023).

[28] M. M. Sharma, G. Lalazissis, J. König, and P. Ring, Phys. Rev. Lett. **74**, 3744 (1995).

[29] S. A. Fayans, S. V. Tolokonnikov, E. L. Trykov, and D. Zawischa, Nucl. Phys. A **676**, 49 (2000).

[30] H. Nakada and T. Inakura, Phys. Rev. C **91**, 021302(R) (2015).

[31] H. Nakada, Phys. Rev. C **92**, 044307 (2015).

[32] H. Nakada, Phys. Rev. C **100**, 044310 (2019).

[33] P. G. Reinhard and W. Nazarewicz, Phys. Rev. C **103**, 054310 (2021).

[34] M. M. Sharma, G. A. Lalazissis, and P. Ring, Phys. Lett. B **317**, 9 (1993).

[35] U. C. Perera, A. V. Afanasjev, and P. Ring, Phys. Rev. C **104**, 064313 (2021).

[36] P. Ring, Prog. Part. Nucl. Phys. **37**, 193 (1996).

[37] D. Vretenar, A. V. Afanasjev, G. A. Lalazissis, and P. Ring, Phys. Rep. **409**, 101 (2005).

[38] J. Meng, H. Toki, S. G. Zhou, S. Q. Zhang, W. H. Long, and L. S. Geng, Prog. Part. Nucl. Phys. **57**, 470 (2006).

[39] *Relativistic Density Functional for Nuclear Structure*, edited by J. Meng (World Scientific, Singapore, 2016).

[40] J. N. Ginocchio, Phys. Rev. Lett. **78**, 436 (1997).

[41] J. Meng, K. Sugawara-Tanabe, S. Yamaji, and A. Arima, Phys. Rev. C **59**, 154 (1999).

[42] H. Liang, J. Meng, and S. G. Zhou, Phys. Rep. **570**, 1 (2015).

[43] S. G. Zhou, J. Meng, and P. Ring, Phys. Rev. Lett. **91**, 262501 (2003).

[44] K. Y. Zhang *et al.*, At. Data Nucl. Data Tables **144**, 101488 (2022).

[45] L. S. Geng, H. Toki, and J. Meng, Prog. Theor. Phys. **113**, 785 (2005).

[46] D. Peña-Arteaga, S. Goriely, and N. Chamel, Eur. Phys. J. A **52**, 320 (2016).

[47] Z. M. Niu, Y. F. Niu, H. Z. Liang, W. H. Long, T. Nikšić, D. Vretenar, and J. Meng, Phys. Lett. B **723**, 172 (2013).

[48] Z. Y. Wang, Y. F. Niu, Z. M. Niu, and J. Y. Guo, J. Phys. G: Nucl. Part. Phys. **43**, 045108 (2016).

[49] T. Marketin, L. Huther, and G. Martínez-Pinedo, Phys. Rev. C **93**, 025805 (2016).

[50] B. N. Lu, E. G. Zhao, and S. G. Zhou, Phys. Rev. C **85**, 011301(R) (2012).

[51] H. Tao, J. Zhao, Z. P. Li, T. Nikšić, and D. Vretenar, Phys. Rev. C **96**, 024319 (2017).

[52] Z. X. Ren, J. Zhao, D. Vretenar, T. Nikšić, P. W. Zhao, and J. Meng, Phys. Rev. C **105**, 044313 (2022).

[53] P. W. Zhao, J. Peng, H. Z. Liang, P. Ring, and J. Meng, Phys. Rev. Lett. **107**, 122501 (2011).

[54] P. W. Zhao, N. Itagaki, and J. Meng, Phys. Rev. Lett. **115**, 022501 (2015).

[55] Z. P. Li, C. Y. Li, J. Xiang, J. M. Yao, and J. Meng, Phys. Lett. B **717**, 470 (2012).

[56] J. M. Yao, K. Hagino, Z. P. Li, J. Meng, and P. Ring, Phys. Rev. C **89**, 054306 (2014).

[57] N. Paar, T. Nikšić, D. Vretenar, and P. Ring, Phys. Rev. C **69**, 054303 (2004).

[58] H. Z. Liang, N. Van Giai, and J. Meng, Phys. Rev. Lett. **101**, 122502 (2008).

[59] Z. M. Niu, Y. F. Niu, H. Z. Liang, W. H. Long, and J. Meng, Phys. Rev. C **95**, 044301 (2017).

[60] X. X. Sun and S. G. Zhou, in *Handbook of Nuclear Physics*, edited by I. Tanihata, H. Toki, and T. Kajino (Springer, Singapore, 2022).

[61] J. Meng and P. Ring, Phys. Rev. Lett. **77**, 3963 (1996).

[62] J. Meng, Nucl. Phys. A **635**, 3 (1998).

[63] J. Meng and P. Ring, Phys. Rev. Lett. **80**, 460 (1998).

[64] J. Meng, H. Toki, J. Y. Zeng, S. Q. Zhang, and S. G. Zhou, Phys. Rev. C **65**, 041302(R) (2002).

[65] X. W. Xia, Y. Lim, P. W. Zhao, H. Z. Liang, X. Y. Qu, Y. Chen, H. Liu, L. F. Zhang, S. Q. Zhang, Y. Kim, and J. Meng, At. Data Nucl. Data Tables **121–122**, 1 (2018).

[66] S. G. Zhou, J. Meng, P. Ring, and E. G. Zhao, Phys. Rev. C **82**, 011301(R) (2010).

[67] L. Li, J. Meng, P. Ring, E. G. Zhao, and S. G. Zhou, Phys. Rev. C **85**, 024312 (2012).

[68] L. L. Li, J. Meng, P. Ring, E. G. Zhao, and S. G. Zhou, Chin. Phys. Lett. **29**, 042101 (2012).

[69] X. X. Sun, J. Zhao, and S. G. Zhou, Phys. Lett. B **785**, 530 (2018).

[70] X. X. Sun, J Zhao, and S. G. Zhou, Nucl. Phys. A **1003**, 122011 (2020).

[71] Z. H. Yang *et al.*, Phys. Rev. Lett. **126**, 082501 (2021).

[72] X. X. Sun, Phys. Rev. C **103**, 054315 (2021).

[73] X. X. Sun and S. G. Zhou, Phys. Rev. C **104**, 064319 (2021).

[74] X.-X. Sun and S.-G. Zhou, Sci. Bull. **66**, 2072 (2021).

[75] S. Y. Zhong, S. S. Zhang, X. X. Sun, S. G. Zhou, and M. S. Smith, Sci. China Phys. Mech. Astron. **65**, 262011 (2022).

[76] K. Y. Zhang, D. Y. Wang, and S. Q. Zhang, Phys. Rev. C **100**, 034312 (2019).

[77] Y. B. Choi, C. H. Lee, M. H. Mun, and Y. Kim, Phys. Rev. C **105**, 024306 (2022).

[78] S. Kim, M. H. Mun, M. K. Cheoun, and E. Ha, Phys. Rev. C **105**, 034340 (2022).

[79] E. J. In, P. Papakonstantinou, Y. Kim, and S. W. Hong, Int. J. Mod. Phys. E **30**, 2150009 (2021).

[80] X. He, C. Wang, K. Zhang, and C. Shen, Chin. Phys. C **45**, 101001 (2021).

[81] K. Y. Zhang, X. He, J. Meng, C. Pan, C. Shen, C. Wang, and S. Zhang, Phys. Rev. C **104**, L021301 (2021).

[82] C. Pan, K. Y. Zhang, P. S. Chong, C. Heo, M. C. Ho, J. Lee, Z. P. Li, W. Sun, C. K. Tam, S. H. Wong, R. W.-Y. Yeung, T. C. Yiu, and S. Q. Zhang, Phys. Rev. C **104**, 024331 (2021).

[83] P. W. Zhao, Z. P. Li, J. M. Yao, and J. Meng, Phys. Rev. C **82**, 054319 (2010).

[84] K. Y. Zhang *et al.* (DRHBc Mass Table Collaboration), Phys. Rev. C **102**, 024314 (2020).

[85] C. Pan *et al.* (DRHBc Mass Table Collaboration), Phys. Rev. C **106**, 014316 (2022).

[86] X. M. Hua, T. H. Heng, Z. M. Niu, B. H. Sun, and J. Y. Guo, Sci. China Phys. Mech. Astron. **55**, 2414 (2012).

[87] W. Sun, K. Y. Zhang, C. Pan, X. H. Fan, S. Q. Zhang, and Z. P. Li, Chin. Phys. C **46**, 064103 (2022).

[88] T. Nikšić, Z. P. Li, D. Vretenar, L. Prochniak, J. Meng, and P. Ring, Phys. Rev. C **79**, 034303 (2009).

[89] Z. P. Li, T. Nikšić, D. Vretenar, J. Meng, G. A. Lalazissis, and P. Ring, Phys. Rev. C **79**, 054301 (2009).

[90] P. Bonche, J. Dobaczewski, H. Flocard, P. H. Heenen, and J. Meyer, Nucl. Phys. A **510**, 466 (1990).

[91] J. Libert, M. Girod, and J. P. Delaroche, Phys. Rev. C **60**, 054301 (1999).

[92] L. Próchniak, P. Quentin, D. Samsoen, and J. Libert, Nucl. Phys. A **730**, 59 (2004).

[93] X. Y. Wu and J. M. Yao, Phys. Rev. C **99**, 054329 (2019).

[94] K. Q. Lu, Z. X. Li, Z. P. Li, J. M. Yao, and J. Meng, Phys. Rev. C **91**, 027304 (2015).

[95] Y. L. Yang, Y. K. Wang, P. W. Zhao, and Z. P. Li, Phys. Rev. C **104**, 054312 (2021).

[96] M. Hemalatha, A. Bhagwat, A. Shrivastava, S. Kailas, and Y. K. Gambhir, Phys. Rev. C **70**, 044320 (2004).

[97] R. Rodríguez-Guzmán, P. Sarriguren, L. M. Robledo, and S. Perez-Martin, Phys. Lett. B **691**, 202 (2010).

[98] J. Xiang, Z. P. Li, Z. X. Li, J. M. Yao, and J. Meng, Nucl. Phys. A **873**, 1 (2012).

[99] A. Gade *et al.*, Phys. Rev. Lett. **95**, 022502 (2005).

[100] E. Clément *et al.*, Phys. Rev. Lett. **116**, 022701 (2016).

[101] S. Cruz *et al.*, Phys. Lett. B **786**, 94 (2018).

[102] S. Cruz *et al.*, Phys. Rev. C **100**, 054321 (2019).

[103] P. Singh *et al.*, Phys. Rev. Lett. **121**, 192501 (2018).

[104] Y. Fu, H. Mei, J. Xiang, Z. P. Li, J. M. Yao, and J. Meng, Phys. Rev. C **87**, 054305 (2013).

[105] E. Maya-Barbecho and J. E. García-Ramos, Phys. Rev. C **105**, 034341 (2022).

[106] H. Mei, J. Xiang, J. M. Yao, Z. P. Li, and J. Meng, Phys. Rev. C **85**, 034321 (2012).

[107] S. Verma, P. A. Dar, and R. Devi, Phys. Rev. C **77**, 024308 (2008).

[108] D. A. Sazonov, E. A. Kolganova, T. M. Shneidman, R. V. Jolos, N. Pietralla, and W. Witt, Phys. Rev. C **99**, 031304(R) (2019).

[109] T. Togashi, Y. Tsunoda, T. Otsuka, and N. Shimizu, Phys. Rev. Lett. **117**, 172502 (2016).

[110] S. Miyahara and H. Nakada, Phys. Rev. C **98**, 064318 (2018).

[111] N. Gavrielov, A. Leviatan, and F. Iachello, Phys. Rev. C **105**, 014305 (2022).

[112] E. V. Mardyban, E. A. Kolganova, T. M. Shneidman, and R. V. Jolos, Phys. Rev. C **105**, 024321 (2022).

[113] S. G. Zhou, J. Meng, and P. Ring, Phys. Rev. C **68**, 034323 (2003).

[114] K. Y. Zhang, C. Pan, and S. Q. Zhang, Phys. Rev. C **106**, 024302 (2022).

[115] H. Kucharek and P. Ring, Z. Phys. A **339**, 23 (1991).

[116] J. L. Friar and J. W. Negele, Adv. Nucl. Phys. **8**, 219 (1975).

[117] H. Kurasawa and T. Suzuki, Prog. Theor. Exp. Phys. **2019**, 113D01 (2019).

[118] M. Girod and B. Grammaticos, Nucl. Phys. A **330**, 40 (1979).

[119] D. R. Inglis, Phys. Rev. **103**, 1786 (1956).

[120] S. Beliaev, Nucl. Phys. **24**, 322 (1961).

[121] M. Wang, G. Audi, F. G. Kondev, W. J. Huang, S. Naimi, and X. Xu, Chin. Phys. C **41**, 030003 (2017).

[122] B. Pritychenko, M. Birch, B. Singh, and M. Horoi, At. Data Nucl. Data Tables **107**, 1 (2016).

[123] S. E. Agbemava, A. V. Afanasjev, D. Ray, and P. Ring, Phys. Rev. C **89**, 054320 (2014).

[124] A. Bohr and B. R. Mottelson, *Nuclear Structure* (World Scientific, New York, 1970).